Solution Phase Synthesis of Cu(OH)2 Nanoribbons by Coordination Self-Assembly Using Cu2S Nanowires as Precursors

3 AUTHORS, INCLUDING:

Weixin Zhang
Hefei University of Technology
105 PUBLICATIONS **2,495** CITATIONS

Shihe Yang
The Hong Kong University of Science and Tec…
381 PUBLICATIONS **11,338** CITATIONS

Solution Phase Synthesis of Cu(OH)$_2$ Nanoribbons by Coordination Self-Assembly Using Cu$_2$S Nanowires as Precursors

Xiaogang Wen, Weixin Zhang, and Shihe Yang*

Department of Chemistry, Institute of Nano Science and Technology, The Hong Kong University of Science and Technology, Clear Water Bay, Kowloon, Hong Kong

Zu Rong Dai and Zhong Lin Wang*

Schools of Materials Science and Engineering, Georgia Institute of Technology, Atlanta, Georgia 30332-0245

ABSTRACT

Nanoribbons of Cu(OH)$_2$ have been synthesized by coordination self-assembly in solution. Techniques of XRD, TEM, HRTEM, SEM, ED, EDX, and XPS have been used to characterize the morphology, structure, and composition of the nanoribbons. The Cu(OH)$_2$ nanoribbons are 20–100 nm in width, several nm in thickness, and up to 100 μm in length. The basic building blocks of the coordination self-assembly are the square planar complexes of Cu^{2+}, which are continuously supplied in a controlled manner from the Cu$_2$S nanowires. NH$_3$ serves as a molecular transporter in the nanoribbon assembly process. The advantages of our method for the nanoribbon synthesis lie in the low temperature and mild reaction conditions, which permit large scale production at low cost.

Introduction. One-dimensional (1D) materials (nanowires, nanotubes, nanobelts, and nanoribbons) have been the focus of considerable interest because of their fundamental importance and potential applications in areas such as nanodevices. Many methods have already been developed for the fabrication of 1D materials. Among these methods, many are based on high-temperature processes such as vapor−liquid−solid (VLS) growth,[1−6] laser ablation,[7,8] and vapor−solid (VS) reaction.[9] Other methods exploit the confined spaces of hard templates, e.g., alumina,[10] track-etching polycarbonate membrane,[11,12] calix[4]hydroquinone nanotubes,[13] silica,[14] Cr$_2$GaN,[15] mica,[16] and soft templates, e.g., liquid crystal,[17] reverse micelle,[18] surfactant templates.[19−21]

In recent years, low-temperature growth of nanowires without templates has been reported. Buhro et al. have grown InP nanowires by a solution−liquid−solid (SLS) process.[22] Nanowires of Ag[23] and Se[24,25] have been synthesized in solution by Xia et al. Using a hydrothermal method, Qian's group has synthesized CdS[26] and Mg(OH)$_2$[27] nanorods. Recently, we have also synthesized Cu$_2$S nanowire arrays at r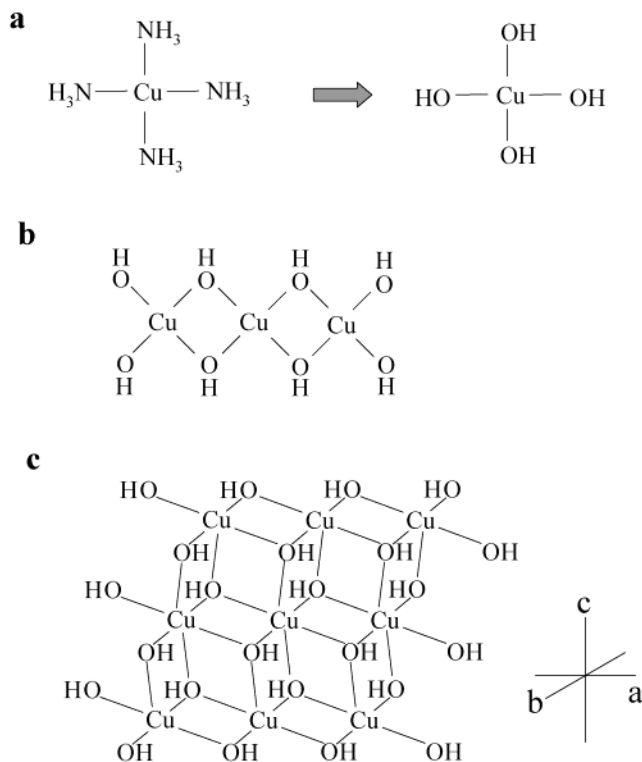oom temperature by gas−solid reaction.[28,29] These methods have potential advantages of relatively low cost, high purity, and large-scale production.

Accompanying the advance in nanowire growth technology is the growing interest in the control of the nanowire morphology. In addition to the cylindrical nanowires, nanocables,[30,31] nanotubes,[32,33] nanocones,[34] nanoneedles,[35] nanostrips,[36] nanoribbons,[37−40] and nanobelts[8,41,42] have also been fabricated at high temperatures.

Here we report the first coordination self-assembly of Cu-(OH)$_2$ nanoribbons in an aqueous solution without any surfactant. Cu(OH)$_2$ is a layered material, and its orthorhombic crystal structure may prove to be ideal for the assembly of nanoribbons. The idea is schematized in Scheme 1. As is well known, Cu^{2+} prefers square planar coordination by OH$^-$ (a), and this leads to an extended chain (b). The chains can be connected through the coordination of OH$^-$ to d$_{z^2}$ of Cu^{2+}, forming a two-dimensional (2D) structure (c). Finally, the 2D layers are stacked through the relatively weak hydrogen bond interactions, and become a three-dimensional (3D) crystal. A key point is that under the right conditions, the crystal growth rate is expected to be quite different,[43] which is the basis for the fabrication of the Cu(OH)$_2$ nanoribbons. In this work, Cu$_2$S nanowire arrays with

* Corresponding author. E-mail: chsyang@ust.hk

Scheme 1. Schematic Showing the Coordination Assembly Growth of Cu(OH)₂ Nanoribbons

a

H₃N—Cu—NH₃ (with NH₃ above and NH₃ below) ⟹ HO—Cu—OH (with OH above and OH below)

b

(structure showing Cu atoms bridged by OH groups)

c

(layered structure showing Cu atoms with HO and OH groups, with crystallographic axes a, b, c shown)

Figure 1. XRD patterns of (A) pure Cu₂S nanowires on Cu foil before the growth of Cu(OH)₂ nanoribbons; (B) Cu(OH)₂ nanoribbons and the remaining Cu₂S nanowires on Cu foil; and (C) pure Cu(OH)₂ nanoribbons after separation.
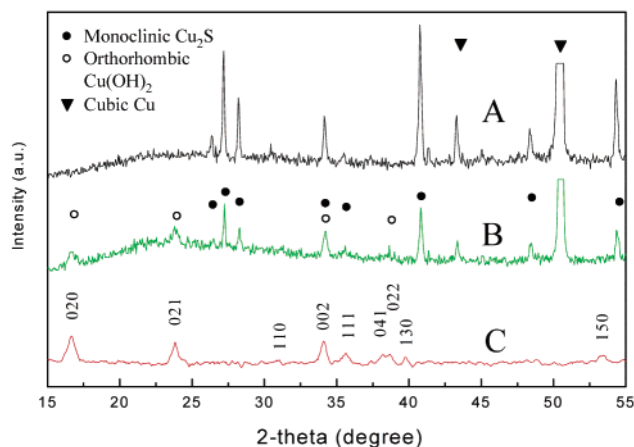
a large surface area and open structure were used as a controlled delivery source of Cu²⁺ for the nanoribbon assembly in an aqueous solution under oxidative and alkaline conditions. Cu²⁺ was then transported to the assembly sites by NH₃ in the form of coordination complexes.

Experimental Section. The synthesis of Cu₂S nanowires on copper surfaces has been described previously (O₂/H₂S = 1.0; reaction time: 10 h).[29] Before the preparation of Cu(OH)₂ nanoribbons, the Cu₂S nanowires were washed with an aqueous solution of HCl (1.0 M) for ~20 min and subsequently with deionized water three times to remove surface impurities. The Cu₂S nanowires on a copper foil were then immersed into an aqueous solution of ammonia (Aldrich, 0.01 M, pH = 9−10). After reacting for 2 h, a blue layer formed on the surface of the substrate. Finally, the samples were taken out of the reactor after a given reaction time, washed with deionized water three times, and dried in air.

Scanning electron microscopy (SEM) of the samples was carried out using JEOL 6300 at an accelerating voltage of 15 kV. For transmission electron microscopy (TEM, Hitachi HF-2000 FEG and Philips-CX20 at 200 kV, and JEOL 4000EX at 400 kV) characterization, the Cu₂S nanowires and Cu(OH)₂ nanoribbons were grown on Cu grids directly. X-ray diffraction (XRD) spectra of the samples were taken on a powder X-ray diffractometer (Philips PW-1830).

Results and Discussion. Shown in Figure 1 are XRD spectra of the samples before (A) and after (B) the nanoribbon growth reaction. Before reaction, only the as-prepared Cu₂S phase appeared (Figure 1A). New peaks showed up after reacting for 48 h (Figure 1B), indicating the formation

of orthorhombic Cu(OH)₂. At the same time, the diffraction peaks of the monoclinic Cu₂S, albeit still present, were reduced significantly in their intensities after reaction. According to the XRD spectrum (Figure 1B), the cell parameters of Cu(OH)₂ are calculated to be: $a = 2.9791$ Å, $b = 10.5417$ Å, and $c = 5.2599$ Å, which are in good agreement with the literature values of bulk Cu(OH)₂ ($a = 2.9471$ Å, $b = 10.5930$ Å, and $c = 5.2564$ Å). A conspicuous feature of the Cu(OH)₂ diffraction peaks is their broadness, which indicates the small size of the Cu(OH)₂ crystals. The average size of the Cu(OH)₂ crystals has been estimated to be 12 nm by the Debye−Scherrer equation ($B = 0.89\lambda/(D\cos\theta)$). This is consistent with the TEM results as will be described below. The blue Cu(OH)₂ layer could be separated from the black Cu₂S layer by applying a small lateral force. The XRD pattern of the blue Cu(OH)₂ sample after separation is shown as the spectrum C in Figure 1. It exhibits almost only the Cu(OH)₂ diffraction peaks, demonstrating the effect of sample separation.
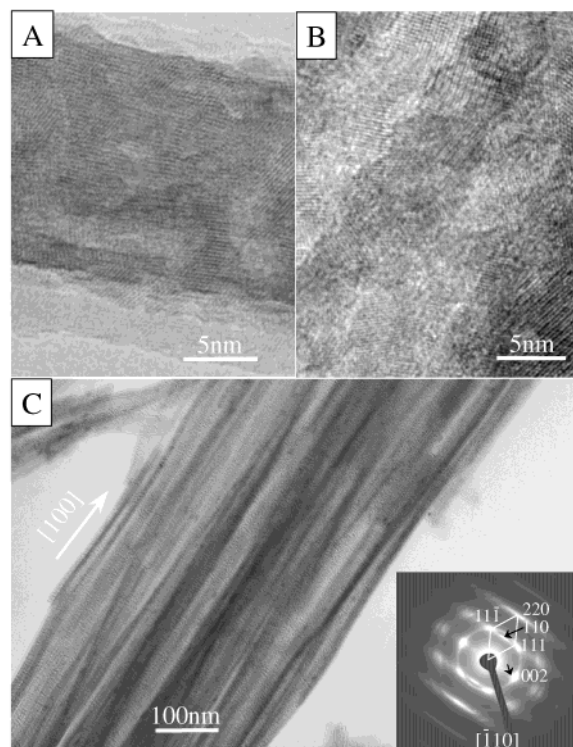
Figure 2A presents a low magnification TEM image of the Cu(OH)₂ sample. It appears that the sample consists entirely of very long ribbon-like nanostructures with a relatively uniform width (~20−100 nm) and sharp boundary on this scale. The ribbon morphology can be appreciated from the thinning in the smooth bend and wring sections indicated with black and white arrows in Figure 2A and the black arrow in Figure 2B; this thinning would not occur for cylindrical nanowires. The inset of Figure 2A shows a select area electron diffraction (SAD) pattern taken from the region including lots of nanoribbons, in which the primary ring pattern, diffraction induced by polycrystal, can be indexed with the orthorhombic Cu(OH)₂. The diffraction intensity is, however, not uniform over some rings, indicating the existence of preferential orientation or texture structure in the Cu(OH)₂ nanoribbons. Higher magnification TEM images (Figure 2B,C) show that the ribbon-like Cu(OH)₂ is either single nanoribbon with the typical width of ~20−100 nm (Figure 2C) or a bundle of the single nanoribbons, as indicated by white arrows in Figure 2B. In comparison to the single nanoribbon, the bundled nanoribbons usually have
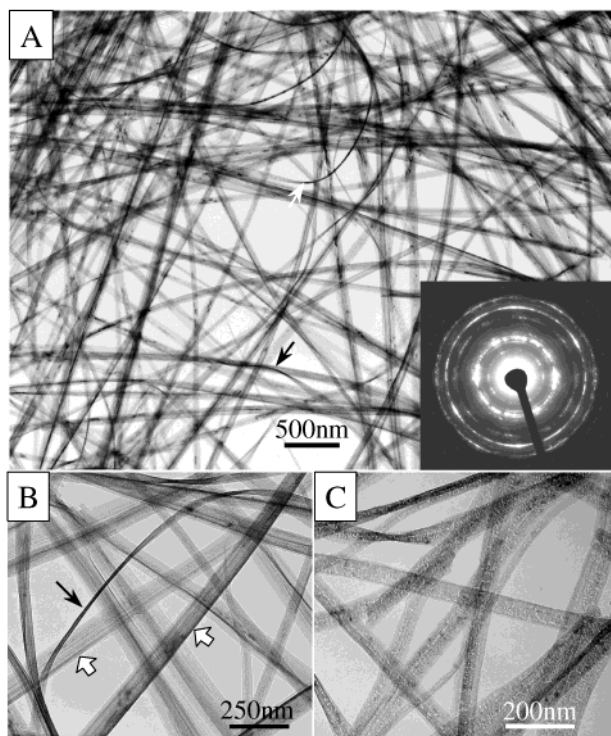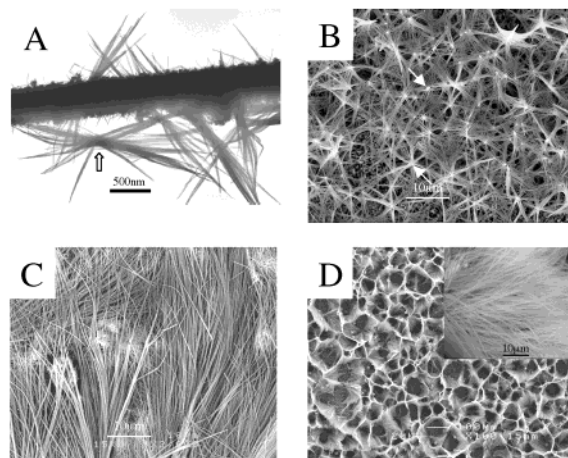
Figure 2. TEM images of Cu(OH)$_2$ nanoribbons at different magnifications. Inset of (A): ED pattern taken from the region including many Cu(OH)$_2$ nanoribbons.

Figure 3. HRTEM images of a single nanoribbon of Cu(OH)$_2$ (A) and a bundle of nanoribbons (B). (C) A TEM image of bundled Cu(OH)$_2$ nanoribbons. Inset of (C): ED pattern of the bundled Cu-(OH)$_2$ nanoribbons.

Figure 4. TEM and SEM images of Cu(OH)$_2$ nanoribbons after different growth times. (A) TEM image after 0.5 h; (B) SEM image after 4 h; (C) SEM image after 3 days; (D) SEM image after 7 days. Inset of (D): higher magnification.

a wider width from several tens (Figure 2B) up to several hundred (Figure 3C) nanometers. The thickness of the Cu-(OH)$_2$ nanoribbons can be estimated to be smaller than 10 nm from the TEM image (Figure 2B). Cavities or holes have been seen to distribute uniformly over the nanoribbons (Figure 2B,C).

Shown in Figure 3A,B are high-resolution transmission electron microscopy (HRTEM) images of the single and a bundled Cu(OH)$_2$ nanoribbon, respectively. Evidently, both types of Cu(OH)$_2$ nanoribons are not single crystalline. The crystallites with different orientations can be distinguished. The boundaries between the single nanoribbons can be clearly seen from the image (Figure 3B), indicating that the bundled nanoribbons are likely produced in the form of intergrowth of single nanoribbons rather than mechanical overlapping. Although the nanoribbons are polycrystalline, orientations of the crystallites are not random but coordinated, in evidence of the electron diffraction pattern (the inset of Figure 3C) corresponding to a bundled nanoribbon (Figure 3), where some very strong reflections can be seen, although they are quite diffuse. A striking scattering feature induced by the boundary effect is also identified, which is perpendicular to the axial direction of the bundled nanoribbons. Some of the reflections are indexed matching the [$\bar{1}$10] zone of the orthorhombic Cu(OH)$_2$, as labeled in the diffraction pattern. Crystallographic analysis indicates that the growth direction is very closed to the [100] in average, and a single nanoribbon is enclosed with the (010) and the (001) as side and top planes. As a result, the nanoribbons are not single crystalline, but the crystallites composed do not randomly connected together, instead the crystallites tend to orient their

[100] crystal direction to be parallel to axis direction of Cu-(OH)$_2$ nanoribbon, and their (010) and (001) crystal planes to parallel to the enclosed surface of the nanoribbons on average.

To gain a better understanding of the mechanism of the nanoribbon growth, we have studied the time course of the reaction by TEM and SEM. Figure 4 shows TEM (A) and SEM (B, C, and D) images of Cu(OH)$_2$ nanoribbons obtained after different reaction times. After reacting for 0.5 h (Figure 4A), nanoribbons can be seen around the Cu$_2$S nanowires,

but they are sparse and short (2.5 μm). Note that these nanoribbons were not grown from the Cu$_2$S nanowires directly. Most Cu(OH)$_2$ nanoribbon bundles appear like a sheaf of straw tied in the middle (see arrow in Figure 4A). This suggests that the nucleation of the nanoribbons occurred at the tied region, and the growth fronts radiated in opposite directions. As the reaction time was increased to 4.0 h (Figure 4B), the nanoribbons were grown much longer ($\sim$20 μm), and a hexagonal-like network of nanoribbons covered the Cu$_2$S nanowire arrays. The radial growth pattern of the Cu-(OH)$_2$ nanoribbons is clearly discernible. In addition, at nanoribbon radiation centers, Cu$_2$S nanowire tips can be seen (see arrows in Figure 4B). Conceivably, the concentrations of Cu^{2+} are higher at these points, a condition that is favorable for the nucleation of the Cu(OH)$_2$ nanoribbons. Panel C of Figure 4 shows an SEM image of nanoribbons obtained after reaction for 3 days. The uniform Cu(OH)$_2$ nanoribbons become much longer ($\sim$70 μm), and still lie down on the substrate. An SEM image of the Cu(OH)$_2$ nanoribbons grown with a 7-day reaction time is shown in panel D of Figure 4. Here, the Cu(OH)$_2$ nanoribbons are even longer ($\sim$100 μm) and have completely covered the Cu$_2$S nanowire arrays. As the nanoribbons become longer, they start to grow vertically, and finally form a honeycomb-like structure. Inside the honeycomb, features shown in Figure 4B are observed. This morphology may be related to interplay between the Cu^{2+} release pattern, the nanoribbon growth rate, and the attendant hydrodynamics at the microscopic scale.

We now come back to the growth mechanism of the Cu-(OH)$_2$ nanoribbons as illustrated in Scheme 1. First of all, the Cu^{2+} cations come from the oxidation of the Cu$_2$S nanowires under the basic condition (e.g., Cu$_2$S $\rightarrow$ CuS + Cu; Cu + O$_2$ $\rightarrow$ Cu^{2+}) and exist in the form of [Cu(NH$_3$)$_4$]$^{2+}$. The Cu(OH)$_2$ nanoribbon assembly results from the following equilibrium:

$$[Cu(NH_3)_n]^{2+} = [Cu(NH_3)_{n-1}(OH)]^+ =$$
$$[Cu(NH_3)_{n-2}(OH)_2] = [Cu(OH)_n]^{(n-2)-}$$
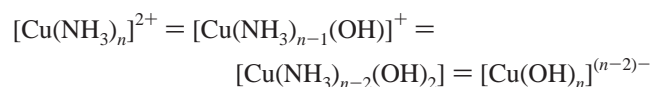
It is plausible that the nucleation of Cu(OH)$_2$ starts from localized regions with relatively high concentrations of [Cu-(NH$_3$)$_n$]$^{2+}$. Once the nucleus is formed, the assembly Cu-(OH)$_2$ nanoribbons can start on it. As mentioned above, the growth rate is quite different along different directions. We believe that the >Cu(OH)$_2$···Cu(OH)$_2$Cu< chain is the fastest growing direction and it is therefore the nanoribbon direction ([100]). For the nanoribbon assembly, the molecular transport complex [Cu(NH$_3$)$_n$(H$_2$O)$_m$(OH)$_l$]$^{(2-l)+}$ is very important; it transports Cu^{2+} to the growing nanoribbon tips with OH$^-$ ligands attached. The attachment of the complex is likely accompanied by the release of NH$_3$ ligands. Continuous assembly in this way yields a long chain, and further assembly of many such chains will then form the nanoribbons.

There remains an important question: why are the assembled Cu(OH)$_2$ nanoribbons more like polycrystalline? To answer this question, one has to examine how the >Cu-

(OH)$_2$Cu< chains are combined. It is likely that some NH$_3$ ligands are trapped between the chains, which may provide sites for defect growth. However, we have failed to detect the N element by XPS. Another possibility is that the Cu-(OH)$_2$ nanoribbon framework is single crytsalline, but the surfaces are covered with many small nanocrystals that mask the single crystalline structure of the nanoribbon core.

Conclusions. In summary, we have successfully synthesized Cu(OH)$_2$ nanoribbons that are 20−100 nm in width, several nm in thickness, and up to 100 μm in length by a simple solution-phase process. Our method relies on the coordination self-assembly of the square planar complexes of Cu^{2+}, which are continuously supplied in a controlled manner from the Cu$_2$S nanowires. NH$_3$ seems to play an important role in the nanoribbon assembly process as a material transporter. The advantages of our method for the nanoribbon synthesis lie in the low temperature and mild reaction conditions, which permit large scale production at low cost. The Cu(OH)$_2$ nanoribbons have a flexible and loose structure, and therefore may lend themselves to be precursors for the fabrication of other copper-based (e.g., CuO) low-dimensional materials. These low-dimensional materials in general promise many potential applications in sensory devices, catalysis, and superconductors.

References

(1) Duan, X. F.; Lieber, C. M. *Adv. Mater.* **2000**, *12*, 298.
(2) Hu, J. T.; Odom, T. W.; Lieber, C. M. *Acc. Chem. Res.* **1999**, *32*, 435.
(3) Pan, Z. W.; Dai, Z. R.; Ma, C.; Wang, Z. L. *J. Am. Chem. Soc.* **2002**, *124*, 1817.
(4) Huang, M. H.; Wu, Y. Y.; Feick, H.; Tran, N.; Weber, E.; Yang, P. D. *Adv. Mater.* **2001**, *13*, 113.
(5) Liang, C. H.; Meng, G. W.; Lei, Y.; Phillipp, F.; Zhang, L. D. *Adv. Mater.* **2001**, *13*, 1330.
(6) Wu, Y. Y.; Yang, P. D. *Chem. Mater.* **2000**, *12*, 605.
(7) Morales, A. M.; Lieber, C. M. *Science* **1998**, *279*, 208.
(8) Zhang, Y. F.; Tang, Y. H.; Wang, N.; Yu, D. P.; Lee, C. S.; Bello, I.; Lee, S. T. *Appl. Phys. Lett.* **1998**, *72*, 1835.
(9) Pan, Z. W.; Dai, Z. R.; Wang, Z. L. *Science* **2001**, *291*, 1947.
(10) Cao, H. Q.; Xu, Z.; Sang, H.; Sheng, D.; Tie, C. Y. *Adv. Mater.* **2001**, *13*, 121.
(11) Jirage, K. B.; Hulteen, J. C.; Martin, C. R. *Science* **1997**, *278*, 655.
(12) Martin, C. R. *Science* **1994**, *266*, 1961.
(13) Hong, B. H.; Bae, S. C.; Lee, C. W.; Jeong, S.; Kim, K. S. *Science* **2001**, *294*, 348.
(14) Huang, M. H.; Choudrey, A.; Yang, P. D. *Chem. Commun.* **2000**, 1063.
(15) Barsoum, M. W.; Farber, L. *Science* **1999**, *284*, 937.
(16) Sun, L.; Searson, P. C.; Chien, C. L. *Phys. Rev.* **2000**, *61*, 6463.
(17) Huang, L. M.; Wang, H. T.; Wang, Z. B.; Mitra, A.; Zhao, D. Y.; Yan, Y. S. *Chem. Mater.* **2002**, *14*, 876.
(18) Qi, L. M.; Ma, J. M.; Cheng, H. M.; Zhao, Z. G. *J. Phys. Chem. B* **1997**, *101*, 3460.
(19) Murphy, C. J.; Jana, N. R. *Adv. Mater.* **2002**, *14*, 80.
(20) Wang, W. Z.; Wang, G. H.; Wang, X. S.; Zhan, Y. J.; Liu, Y. K.; Zheng, C. L. *Adv. Mater.* **2002**, *14*, 67.
(21) Rees, G. D.; Gowing, R. E.; Hammond, S. J.; Robinson, B. H. *Langmuir* **1999**, *15*, 1993.
(22) Trentler, T. J.; Hickman, K. M.; Goel, S. C.; Viano, A. M.; Gibbons, P. C.; Buhro, W. E. *Science* **1995**, *270*, 1791.
(23) Sun, Y. G.; Xia, Y. N. *Adv. Mater.* **2002**, *14*, 833.
(24) Sun, Y. G.; Gates, B.; Mayers, B.; Xia, Y. N. *Nano. Lett.* **2002**, *2*, 165.

(25) Gates, B.; Yin, Y. D.; Xia, Y. N. *J. Am. Chem. Soc.* **2000**, *122*, 12582.

(26) Hu, J. Q.; Deng, B.; Zhang, W. X.; Tang, K. B.; Qian, Y. T. *Inorg. Chem.* **2001**, *40*, 3130.

(27) Ding, Y.; Zhang, G. T.; Wu, H.; Hai, B.; Wang, L. B.; Qian, Y. T. *Chem. Mater.* **2001**, *13*, 435.

(28) Wang, S. H.; Yang, S. H. *Chem. Phys. Lett.* **2000**, *322*, 567.

(29) Wang, S. H.; Yang, S. H. *Chem. Mater.* **2001**, *13*, 4794.

(30) Shi, W. S.; Peng, H. Y.; Xu, L.; Wang, N.; Tang, Y. H.; Lee, S. T. *Adv. Mater.* **2000**, *12*, 1927.

(31) Ma, R. Z.; Bando, Y.; Sato, T. *Chem. Phys. Lett.* **2001**, *350*, 1.

(32) Wang, Z. L.; Gao, R. P.; Gole, J. L.; Stout, J. D. *Adv. Mater.* **2000**, *12*, 1938.

(33) Ma, R. Z.; Bando, Y.; Sato, T. *Adv. Mater.* **2002**, *14*, 366.

(34) Baylor, L. R.; Merkulov, V. I.; Ellis, E. D.; Guillorn, M. A.; Lowndes, D. H.; Melechko, A. V.; Simpson, M. L.; Whealton, J. H. **2002**, *91*, 4602.

(35) Stoner, B. R.; Cui, H. J. *Mater. Res.* **2001**, *16*, 3111.

(36) Yazami, R.; Gabrisch, H.; Fultz, B. *J. Chem. Phys.* **2001**, *115*, 10585.

(37) Dai, Z. R.; Pan, Z. W.; Wang, Z. L. *Solid State Comm.* **2001**, *118*, 351.

(38) Dai, Z. R.; Pan, Z. W.; Wang, Z. L. *J. Phys. Chem. B* **2002**, *106*, 902.

(39) Hu, J. Q.; Ma, X. L.; Shang, N. G.; Xie, Z. Y.; Wong, N. B.; Lee, C. S.; Lee, S. T. *J. Phys. Chem. B* **2002**, *106*, 3823.

(40) Law, M.; Kind, H.; Messer, B.; Kim, F.; Yang, P. D. Angew. *Chem., Int. Ed.* **2002**, *41*, 2405.

(41) Pan, Z. W.; Dai, Z. R.; Wang, Z. L. *Appl. Phys. Lett.* **2002**, *80*, 309.

(42) Gundiah, G.; Govindaraj, A.; Rao, C. N. R. *Chem. Phys. Lett.* **2002**, *351*, 189.

(43) Clemente, R. R.; Serna, C. J.; Ocana, M.; Matijevic, E. *J. Cryst. Growth* **1994**, *143*, 277.

NL025848V